Modeling changes in hydrate stabilities associated with Arctic warming and its impact on slope instabilities

Khokan Debnath, Dr. Jocelyn L. Hayley, & Dr. Jeffrey A. Priest
Department of Civil Engineering– University of Calgary, Calgary, Alberta, Canada

ABSTRACT
Large volumes of methane hydrate exist within marine sediments across the Arctic region, such as sediments on the continental margin of the Beaufort Sea. The low temperatures and high pressures required for hydrate stability, and the cold water in this region leads to hydrate being formed at comparatively shallower depths relative to other oceanic sediments. Because of global warming, it is estimated that the ocean bottom temperature of the Arctic region has increased by as much as 1ºC since 1979. If this trend in increasing ocean bottom temperature were to continue, hydrate dissociation within the sediment may occur potentially causing slope instabilities. In this paper, changes in the seabed geothermal conditions were modeled to estimate the reduction in the hydrate stability zones within the sediment on the continental margin. The change in sediment strength due to gas hydrate dissociation has been incorporated as input variables in to a slope stability model to determine changes in factor of safety associated with hydrate dissociation and assess the potential for slope instabilities.

RÉSUMÉ
D'importants volumes d'hydrate de méthane existent dans les sédiments marins de la région Arctique, tels que les sédiments sur la marge continentale de la Mer de Beaufort. Les basses températures et les pressions élevées requises pour la stabilité des hydrates et l'eau froide dans cette région conduisent à la formation d'hydrates à des profondeurs relativement plus faibles par rapport aux autres sédiments Océaniques. En raison du réchauffement planétaire, on estime que la température du fond Océanique de la région Arctique a augmenté de plus de 1 °C depuis 1979. Si cette tendance à l'augmentation des températures du fond Océanique se poursuit, une dissociation hydrique pourrait se produire. Dans cet article, les changements dans les conditions géothermiques du fond marin ont été modélisés pour estimer la réduction des zones de stabilité des hydrates dans les sédiments de la marge continentale. La modification de la résistance des sédiments due à la dissociation des hydrates de gaz a été incorporée comme variables d'entrée dans un modèle de stabilité des pentes pour déterminer les changements du facteur de sécurité associés à la dissociation des hydrates et évaluer le potentiel d'instabilité des pentes.

1 INTRODUCTION

Gas hydrate are ice-like crystalline compounds composed of water and gas where gas molecules are enclosed by cages of water molecules. Methane is the most common gas found in gas hydrate. The formation of gas hydrate requires an ample supply of gas and water and appropriate low temperature and high pressure. As such, significant amounts of gas hydrate are found under the permafrost and within offshore sediments within Canada's border (Nixon and Grozic, 2007). It is estimated that 10,000 Gt of methane is trapped in hydrate within the Arctic margins and 74,400 Gt globally (Klauda and Sandler, 2005). In the Arctic, marine gas hydrates are generally formed in water depths greater than ~300 m (Figure 1) and the thickness of the gas hydrate layer may extend from the seafloor down to a sediment depth of few hundred meters depending on the geothermal gradient.

The global surface temperature has increased significantly over the last three decades compared to any other time since 1850. More precisely, the last 30 years from 1983 to 2012 was probably the warmest period for 1400 years in the Northern Hemisphere, with the Intergovernmental Panel for Climate Change (IPCC) projecting that the average increase in global surface temperature will exceed 1.5 °C by the end of the 21st century (high confidence – based on the model RCP 4.5, RCP6.0, and RCP8.5). However, the Arctic region is expected to experience much greater warming than the global mean with a temperature increase of 12 °C based on the RCP 8.5 projection (IPCC., 2014). Climate models have shown that the Arctic may become seasonally ice free by 2050 or even earlier (James et al., 2016). As gas hydrate forms at shallower depths in the Arctic, it will be more sensitive to increases in seafloor temperature which can lead to dissociation of the hydrate (Ruppel and Kessler, 2017).

This paper considers the impact of increasing ocean bottom temperatures over the next 100 years on the behavior of gas hydrate-bearing offshore sediments and the risk that dissociation of the hydrate may have on slope failure. Different conditions such as increase in seafloor temperature, different geothermal gradients, and seafloor slope angle were investigated.

2 GEOTHERMAL MODELING OF AN ARCTIC SLOPE

A typical continental slope in the Arctic Ocean was chosen as the study area for this research. The Arctic Ocean is composed of an extensive shallow continental shelf that extends up to 100 km offshore, a narrow continental slope and a central deep basin. The water depth on the continental shelf reaches up to 100 m near the shelf break with the continental slope having a water depth from 100 to 1500 m with a slope gradient ranging from 0.5º to 5º or 6º (Blasco et al., 2013) before reaching the deep basin. Due to the cold waters of the arctic ocean hydrate formation occurs at ~300 m below sea level where the current seabed temperature is about 0 ºC, with a seafloor slope gradient which is prone to fail upon hydrate dissociation (Vadakkepuliyambatta et al., 2017). Geothermal modeling of the seafloor sediments was conducted for two distinct scenarios of seafloor temperature rise of 3 ºC/100 years and 6 ºC/100 years to determine the change in hydrate stability zone.

3 MODELING PARAMETERS

Thermal propagation in gas hydrate bearing sediments depends on the thermal conductivity (λ), specific heat capacity (C), and the latent heat (L) or enthalpy of fusion of the sediment components. Thermal properties of gas hydrate and gas hydrate bearing sediments and other model parameters are listed in Table 1 and taken from available literature.

Table 1. Thermal properties of individual component of methane hydrate bearing sediment and other parameters.

Parameter	Value
Thermal conductivity of methane hydrate (λ_h) (Muraoka et al., 2014) (Cortes et al., 2009)	0.575 - 0.619 (W/m/K)
Density of methane hydrate at 0 ºC (Muraoka et al., 2014)	925.2 kg/m^3
Specific heat of methane hydrate (Muraoka et al., 2014)	2191 J/kg/K
Thermal conductivity of water (λ_w) (Muraoka et al., 2014)	0.575 (W/m/K)
Specific Heat of water (Muraoka et al., 2014)	4110 J/kg/K
Thermal conductivity of saturated clay (λ_s) (Hamdhan and Clarke, 2010)	1.9 – 2.2 (W/m/K)
Specific heat of clay (Hamdhan and Clarke, 2010)	800 J/kg/K
Porosity of sediment (ϕ) (Taylor et al., 2013)	0.35 – 0.6
Hydrate saturation (S_h) (Rees et al., 2011)	20% - 30%
Slope angle (Blasco et al., 2013)	3º and 6º
Initial seafloor temperature (Blasco et al., 2013)	0 ºC
Geothermal gradient (Jones et al., 1990)	35 ºC/km
Latent heat of dissociation (L) (Rueff et al., 1988)	431.15 j/g
Salinity (Vadakkepuliyambatta et al., 2017)	3.5%
Seawater density	1035 kg/m^3

Thermal conductivity of a material is the ability to transmit heat by conduction. It is the amount of heat energy that flows through a soil mass under a unit temperature gradient through a unit area and thickness (GEO-SLOPE International Ltd., 2009). Thermal conductivity of three phase (methane hydrate, soil, and seawater) sediment (λ) was calculated using the parallel model as follows:

$$\lambda = S_h \phi \lambda_h + (1-\phi)\lambda_s + S_w \phi \lambda_w \quad [1]$$

where, ϕ is the porosity of the sediment. S_h and S_w represent the hydrate and seawater saturation respectively, where $S_h + S_w = 1$ (Muraoka et al., 2014).

Thermal conductivity of methane hydrate is approximately equal to that of water and hence the presence of methane hydrate in water saturated marine sediment does not impact the thermal conductivity (Waite, 2007).

Specific heat is the amount of energy required to increase temperature of an object by one degree for a unit mass. The specific heat of hydrate-bearing marine sediments depends on the mass fraction of sediment, seawater, and methane hydrate. The bulk specific heat of methane hydrate bearing sediment is estimated using the following formula:

$$C_{p.b}\rho_b = C_{p.m}\rho_m(1-\emptyset) + C_{p.w}\rho_w(1-S_h)\emptyset + C_{p.h}\rho_h S_h \emptyset \quad [2]$$

The mass fraction, ρ_b, is given by:

$$\rho_b = \rho_m(1-\emptyset) + \rho_w(1-S_h)\emptyset + \rho_h S_h \emptyset \quad [3]$$

where, $C_{p.b}$ - Bulk specific heat of gas hydrate bearing sediment

ρ_b - Bulk mass fraction of gas hydrate bearing sediment

$C_{p.m}, C_{p.w}, C_{p.h}$ - Specific heat of mineral grain, water, and hydrate, respectively

ρ_m, ρ_w, ρ_h - Mass fraction of sediment grain mineral, seawater, and hydrate, respectively (Waite et al., 2009)

Recent studies indicate that hydrate can from in fine grained sediment, where the hydrate saturation can reach up to between ~ 20% to 30% (Rees et al., 2011). Typically gas hydrate does not form within the top few meters of the seafloor surface due to the presence of sulfate which consumes methane, and hence a 5 m thick sulfate reduction zone, where no hydrate is present, is assigned to accommodate this process (Priest and Grozic, 2016).

It is assumed that hydrate is homogeneously disseminated throughout the stability zone and heat transfer in the soil, water, and gas hydrate takes place by conduction only. A constant geothermal heat flux was assigned to the bottom boundary for each model run since there is no change in geothermal energy source over the 100 years for which a rise in seafloor surface temperature is applied. The depth of the bottom boundary from the seafloor at x=0 is 105 m and reduces with depth downslope according to the chosen slope angle. Geothermal heat flux for a homogeneous soil was calculated using the following formula:

$$Q = -\lambda * G \quad [4]$$

Where, Q - Heat flux in kJ/days/m²
G - Geothermal gradient in ºC/m

Equation [4] is valid for vertical heat flow in a homogeneous media due to conduction (Williams and Smith 2009).

The stability of gas hydrate depends on appropriate pressure and temperature, the type of hydrate, and the presence of inhibitors such as salt. The phase boundary for methane hydrate with 3.5% salinity was determined using the hydrate prediction program “HYDOFF” (Sloan, 1998) and illustrated in Figure 1.

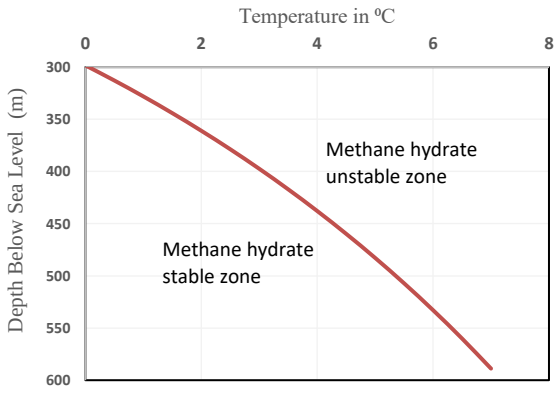

Figure 1. Phase diagram of methane hydrate for 3.5% salinity

Input parameters such as thermal conductivity, volumetric heat capacity, and geothermal flux were calculated using equations [1 – 4] and are listed in Table 2.

Table 2. Parameters for the geothermal numerical model

Model Parameters	Values
λ of GH[1] bearing sediment	134 kJ/day/m/ºC
λ of sediment without GH	134 kJ/day/m/ºC
λ of sulfate reduction zone	106 kJ/day/m/ºC
C_h[2] of GH bearing sediments (Before dissociation)	2,860 kJ/m³/ºC
C_h of GH bearing sediments (Dissociated)	2,960 kJ/m³/°C
C_h of sediments without GH	2,960 kJ/m³/°C
C_h of sediments in 5 m sulfate reduction zone	3,400 kJ/m³/°C
Geothermal flux	4.7 kJ/days/m²

[1] – GH – Gas hydrate
[2] - C_h – Volumetric heat capacity

4 IMPACT OF GEOTHERMAL GRADIENT ON GAS HYDRATE STABILITY ZONE AND DISSOCIATION PATTERN

The extent of the gas hydrate stability zone (GHSZ) and the degree of gas hydrate dissociation that occurs for a given temperature rise depends on the geothermal gradient. Numerous researchers have considered different geothermal gradients to analyze the methane hydrate stability zone in the Arctic. For example, a geothermal gradient of 87 ºC/km was used by Reagan et al. (2011), while a geothermal gradient of 10 ºC/km, 12 ºC/km, 13.8 ºC/km, and 20 ºC/km was utilized by Gorman and Senger (2010) to determine the gas hydrate stability zone.

The geothermal gradient in the Arctic region varies from 15 ºC/km to 50 ºC/km (Majorowicz and Embry, 1998) with the Beaufort Sea area, in particular, varying from 22 – 44 ºC/km (Jones et al., 1990). Thus, the extent of the methane hydrate stability zones was considered for geothermal gradients of 25 ºC/km, 30 ºC/km, 35 ºC/km, and 40 ºC/km and presented in

Figure 2. The results were obtained using TEMP/W, a computer based finite element numerical modeling tool, to determine the temperature of elements under steady state condition for a target geothermal gradient and compared with the temperature and pressure conditions required for hydrate stability.

In our study, the initial GHSZ was determined using a seabed temperature of 0 ºC, and 3º slope angle. The seawater depth at (0,0) point is ~275 m. Annual variation in bottom water temperature were not considered in this analysis. It should be noted that the shape of initial gas hydrate stability zones does not depend on the thermal properties of sediments since a steady state condition was considered.

The geothermal modeling showed that low geothermal gradients resulted in a thick hydrate stability zone that exhibited a defined bulge towards the hydrate free zone. The bulging effect of the stability zones disappears when the geothermal gradient is equal or higher than ~35 ºC/km.

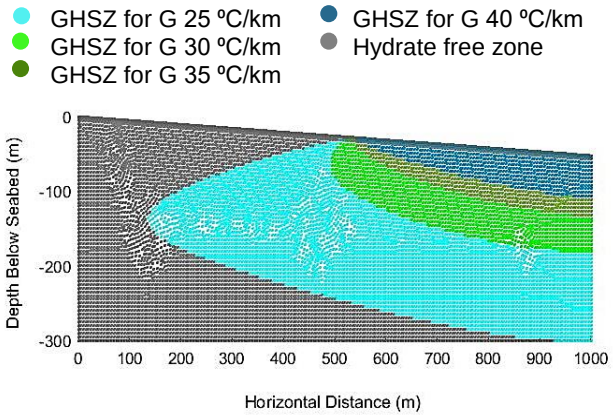

Figure 2. Methane hydrate stability zone (GHSZ) for different geothermal gradients (G). The grey zone represents soil sediments where no hydrate is present.

The most commonly used increase in seafloor temperature that has previously been considered to investigate the change in hydrate stability zone ranges from 1 to 5 ºC. For instances, Reagan et al. (2011) modeled the hydrate stability zone for seafloor temperature increase of 1 ºC, 3 ºC and 5 ºC over a 100 years period. In this research, the increase of seafloor temperature of 3 ºC and 6 ºC was chosen to consider an average and moderately high seafloor temperature change. The impact of the geothermal gradient on gas hydrate stability zone was verified for 3 ºC seafloor temperature increase only. The extent of the gas hydrate dissociated zone (GHDZ) was verified for geothermal gradients of 87 ºC/km, 65 ºC/km, and 35 ºC/km and presented in Figure 3 – 5 respectively. TEMP/W was used to determine the change in temperature for each element at set times over the 100-year period and was compared to the hydrate stability conditions for the given depth and temperature increase to determine the degree of dissociation. For the 87 ºC/km and 65 ºC/km geothermal gradient, the dissociation starts at the tip of the stability wedge and bottom stability boundary and propagates downslope dissociating from top and bottom boundary similar to that observed by Reagan et al. (2011). For the 35 ºC/km geothermal gradient, hydrate dissociation begins at the landward tip of the stability zone and along the top stability boundary with the dissociation front predominantly migrating downwards with increasing time with only minor dissociation occurring along the bottom boundary.

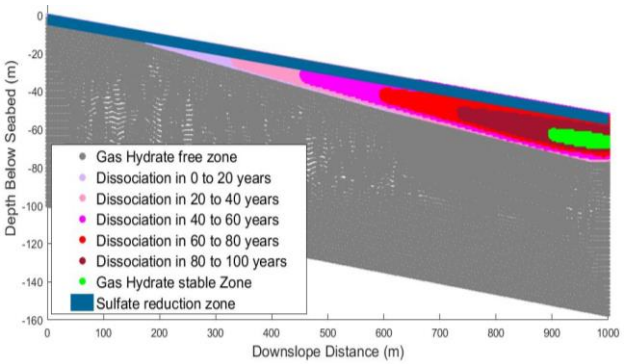

Figure 3. Change in gas hydrate dissociation pattern for a geothermal gradient of 87 ºC/km with 3º slope angle and 3 ºC/ 100 years seafloor temperature rise.

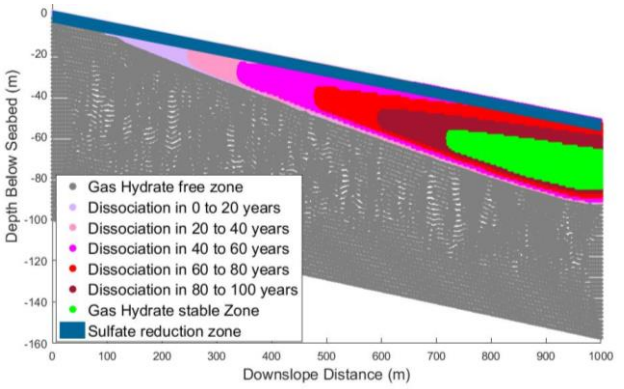

Figure 4. Change in gas hydrate dissociation pattern for a geothermal gradient of 65 ºC/km with 3º slope angle and 3 ºC/ 100 years seafloor temperature rise.

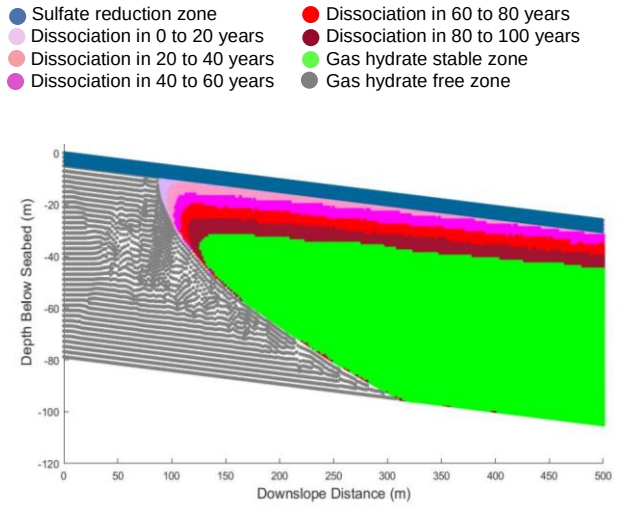

Figure 5. Change in gas hydrate dissociation pattern for a geothermal gradient of 35 ºC/km with 3º slope angle and 3 ºC/ 100 years seafloor temperature rise.

In our study, a geothermal gradient of 35 ºC/km was chosen because it represents an average value in the Beaufort Sea region.

5 RESULTS AND DISCUSSION

5.1 Thermal modeling

The objective of the thermal modeling was to determine the change in the gas hydrate stability zone within the sediment column for defined increases in seafloor temperature for two idealized slope angles over the next 100 years. Four different scenarios were considered as follows:

Model 1: 3º slope angle and 3 ºC/ 100 years seafloor temperature rise.

Model 2: 3º slope angle and 6 ºC/ 100 years seafloor temperature rise.

Model 3: 6º slope angle and 3 ºC/ 100 years seafloor temperature rise.

Model 4: 6º slope angle and 6 ºC/ 100 years seafloor temperature rise.

All the thermal models were analyzed for 20% hydrate saturation and considering discrete 20-year time steps over the 100 year time period. The results for model 1 to 4 are presented in Figures 5-8 respectively with different colors highlighting the degree of dissociation for a given 20-year increment. As expected a similar pattern of hydrate dissociation occurs for all models with dissociation starting at the top of the stability zone with the dissociation front propagating downwards with time. For the models with the steeper slope angle the thickness of the dissociation front becomes thinner with increasing distance downslope because of the increasing hydrostatic pressure.

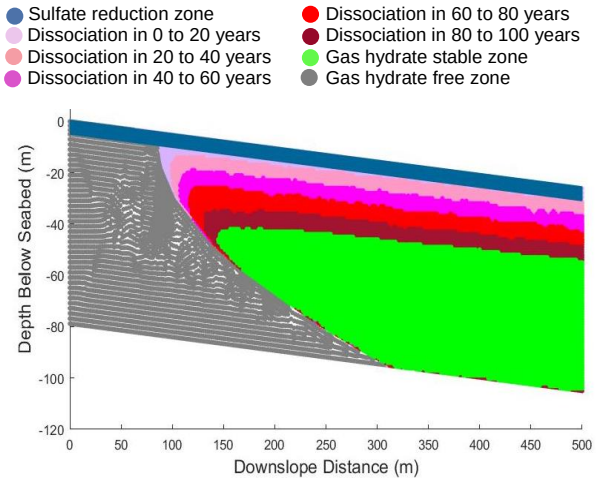

Figure 6. Change in gas hydrate dissociation pattern for a geothermal gradient of 35 ºC/km with 3º slope angle and 6 ºC/ 100 years seafloor temperature rise.

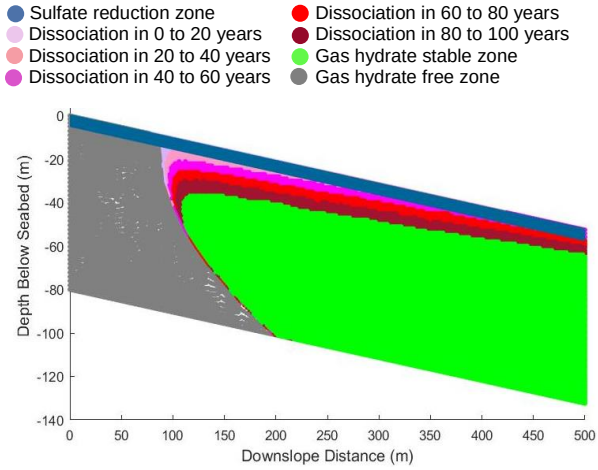

Figure 7. Change in gas hydrate dissociation pattern for a geothermal gradient of 35 ºC/km with 6º slope angle and 3 ºC/ 100 years seafloor temperature rise

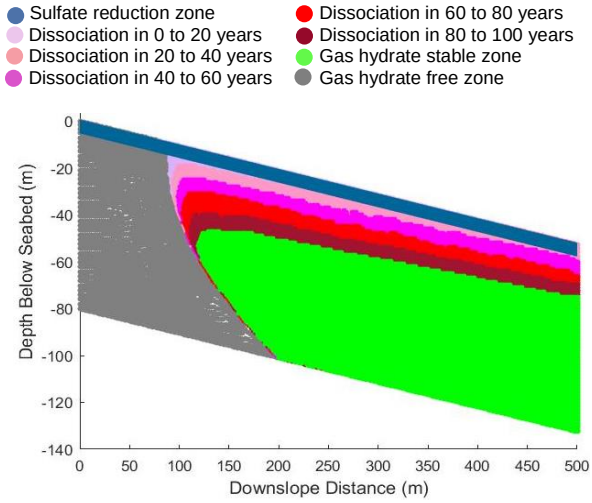

Figure 8. Change in gas hydrate dissociation pattern for a geothermal gradient of 35 ºC/km with 6º slope angle and 6 ºC/ 100 years seafloor temperature rise.

The volume of gas hydrate dissociated for each time step was calculated for each model for a given unit width. The ratio of gas hydrate dissociated volume to the initial gas hydrate volume is plotted against time in Figure *9*. Comparing the results presented in Figure 9, it is found that the greater volumes of hydrate are dissociated for lower slope angles for a given temperature rise.

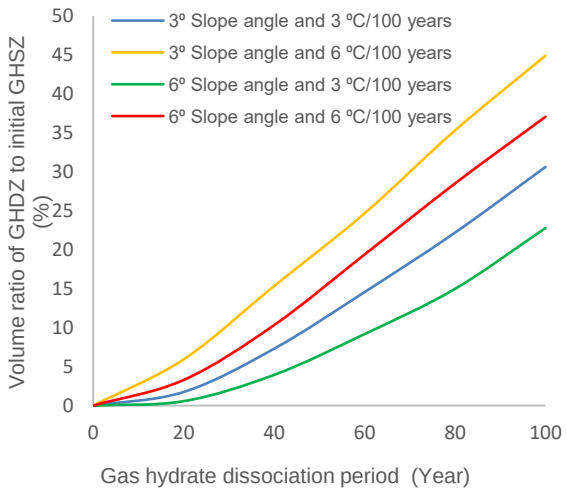

Figure 9. Volume ratio of gas hydrate dissociated zones for 3 ºC and 6 ºC seafloor temperature increase in 100 years and each scenario for 3º and 6º slope angle in different periods. For all scenarios, the porosity (n) is 0.4 and hydrate saturation (S_h) is 20%.

5.2 Slope stability analysis

To consider the impact of hydrate dissociation on slope stability, Models 1-4 were analyzed using the 2-D limit equilibrium slope stability analysis program SLOPE/W (GEO-SLOPE International Ltd., 2017). The slope stability model was run to determine the factor of safety against sliding for each 20-year increment. The analysis was conducted assuming undrained conditions.

The thermal analysis conducted in Section 5.1 assumed that the gas hydrate was disseminated homogeneously throughout the sediment to reduce the complexity of analysis. However, hydrate in fine-grained sediments can exist in fracture-filled heterogeneous sub vertical veins (Rees et al., 2011). The presence of these hydrate veins enhance the strength of sediment matrix by preventing normal consolidation and by supporting the overburden stress (Yun et al., 2010). Hydrate dissociation releases water and gas that increases void ratio and water content, and along with the loss of stiff hydrate acting as a support, leads to an increase in compressibility of the sediment (Kim et al., 2013). In addition, the gas released during dissociation can increase pore pressure and hence reduce effective stresses and lower sediment strength. Tests on sediment matrix where hydrate was previously present show the undrained shear strength, S_u, was significantly lower compared to that expected for hydrate free sediments at the same depths (Priest et al., 2014).

In our modeling, the reduction in effective stress due to release of gas is ignored based on the assumption that excess gas pressure will dissipate along the fractures as hydrate dissociates. Since data regarding the soil strength of hydrate-bearing sediment subject to hydrate dissociation for the Arctic region is not readily available, strength parameters have been taken from published literature listed in Table 3.

Table 3. Sediment strength parameters used in slope stability analysis (Priest and Grozic, 2016).

Soil zone	Undrained shear strength (S_u) kPa	Unit weight kN/m^3
Sulfate reduction zone	8	16.3
Hydrate free zone	6 +0.8 kPa/m	19.4
Dissociated zone	6	19.4

Figure 10 illustrates the failure mass, shape, and the factor of safety for Model 1 at 100 years. The factor of safety has been analyzed for failure paths that only pass through the dissociated zone, since the strength of the hydrate-bearing sediment is assumed to be significantly stronger than the sediment where dissociation was occurring.

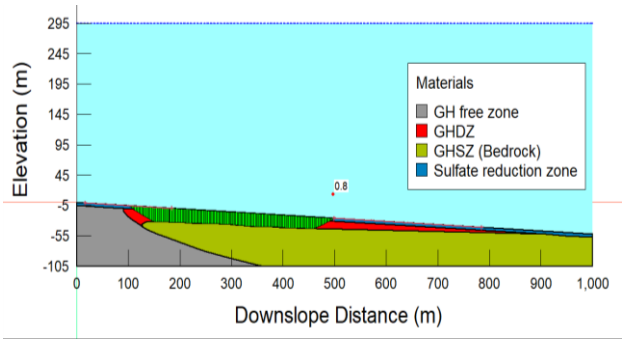

Figure 10. Figure illustrates factor of safety of the dissociated slope in 100 years for the Model 1 with a 3º downslope and 3ºC/100 years seafloor temperature increase. The elevation is positive above and negative below the sea floor.

The results from all four Models illustrate similar patterns regarding the change in factor of safety. Figure 11 highlights the change in factor of safety against time for the different models. For a given rate of seafloor temperature increase, slope failure occurs comparatively earlier when slope angle is higher, even though less volume of hydrate is dissociated. For 3 ºC/100 years seafloor temperature increase and with a 3º slope angle, the slope fails between 75 to 80 years after the onset of warming, where as the 6º slope angle fails between 35 to 40 years after the onset. For a given seafloor slope angle, the slope fails earlier when the rate of seafloor temperature rise is higher. For 3º downslope seafloor angle, the slope fails within 55 to 60 years for a 6 ºC/100 years seafloor temperature increase compared to 75 to 80 years for 3 ºC/100 years seafloor temperature increase.

Model 4 (6 ºC/100 years temperature rise and 6º slope angle) exhibits the shortest duration of 25 to 35 years between onset of the temperature increase and eventual failure of the dissociated hydrate-bearing sediments.

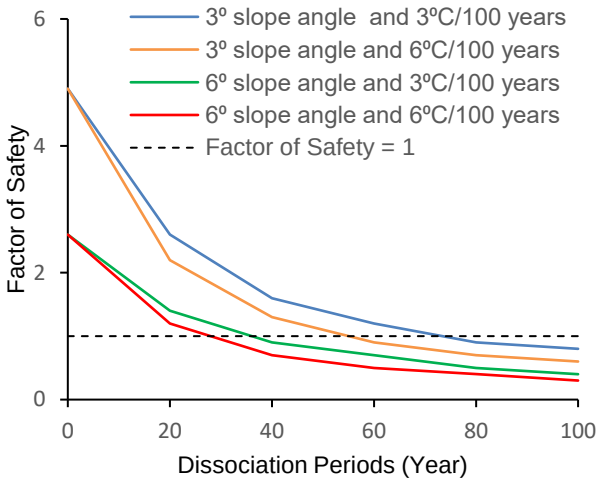

Figure 11. Change in factor of safety for different periods of dissociation for Model 1 to 4.

6 LIMITATIONS

A number of limitations with our modeling approach can be considered:

- Pore pressure increase due to gas hydrate dissociation was not considered in the numerical models and was assumed to dissipate along fractures.
- One of the critical limitations of analyzing gas hydrate bearing sediment using TEMP/W is that the phase change temperature in TEMP/W is a global parameter and hence it cannot be assigned to different layers to incorporate the phase change as a function of depth.

7 CONCLUSION

The predicted increase in Arctic warming will lead to dissociation of gas hydrate and will impact slope stability.

Variations in the geothermal gradient for a given slope will affect the overall volume of the hydrate stability zone and how hydrate dissociation evolves with time. Lower geothermal gradients give rise to a thicker hydrate zone with a distinctive bulge towards the landward hydrate free zone when < 35 ºC/km, whereas higher geothermal gradients produce a wedge like shape and reduced thickness. For low geothermal gradients dissociation starts along the top stability boundary and propagates downwards with time where pressure and temperature overcome the stability condition. However, at a high geothermal gradient hydrate dissociation initially starts along the bottom stability boundary and at the tip of the stability wedge, before extending along the top boundary with increased warming leading to a thinning wedge.

The geothermal modeling shows the volume of the hydrate dissociation zone depends on the rate of increase in seafloor temperature, duration of warming, and the slope angle. The modeling suggests that on the Arctic continental slope hydrate-bearing sediments with a slope angle of 3º will fail in 75 to 80 years for 3 ºC/100 year seafloor temperature increase and in 55 to 60 years for seafloor temperature increase at a rate of 6 ºC/100 years. However, increasing slope angle (6º slope), reduces the time for slope failure to 35 to 40 years and within 25 to 35 years for a 3 ºC/100 year and 6º C/100 year seafloor temperature increase respectively.

References

Blasco, S., Bennett, R., Brent, T., Burton, M., Campbell, P., Carr, E., Covill, R., Dallimore, S., Davies, E., Hughes-Clarke, J., Issler, D., Leonard, L., MacKillop, K., Mazzotti, S., Patton, E., Rogers, G., Shearer, J., and White, M. (2013). *2010 State of Knowledge: Beaufort Sea Seabed Geohazards Associated with Offshore Hydrocarbon Development; Geological Survey of Canada, Open File 6989*. doi:10.4095/292616.

Cortes, D.D., Martin, A.I., Yun, T.S., Francisca, F.M., Santamarina, J.C., and Ruppel, C. 2009. *Thermal conductivity of hydrate-bearing sediments*. Journal of Geophysical Research: Solid Earth, **114**(11): 1–10. doi:10.1029/2008JB006235.

GEO-SLOPE International Ltd. 2017. *Stability Modeling with GeoStudio*. GEO-SLOPE International Ltd., Calgary.

GEO-SLOPE International Ltd. 2009. *Thermal Modeling with TEMP / W 2007*. GEO-SLOPE International Ltd, Calgary.

Gorman, A.R. and Senger, K. 2010. *Defining the updip extent of the gas hydrate stability zone on continental margins with low geothermal gradients*. Journal of Geophysical Research: Solid Earth, **115**(7): 1–8. doi:10.1029/2009JB006680.

Hamdhan, I.N. and Clarke, B.G. 2010. *Determination of Thermal Conductivity of Coarse and Fine Sand Soils*. *In* Proceedings World Geothermal Congress 2010. Bali, Indonesia. pp. 25–29.

IPCC, 2014: Climate Change 2014: Synthesis Report. Contribution of Working Groups I, II and III to the Fifth Assessment Report of the Intergovernmental Panel on Climate Change [Core Writing Team, R.K. Pachauri and L.A. Meyer (eds.)]. IPCC, Geneva, Switzerland, 151 pp.

James, R.H., Bousquet, P., Bussmann, I., Haeckel, M., Kipfer, R., Leifer, I., Niemann, H., Ostrovsky, I., Piskozub, J., Rehder, G., Treude, T., Vielstadte, L., and Greinert, J. 2016. *Effects of climate change on methane emissions from seafloor sediments in the Arctic Ocean: A review*. Limnology and Oceanography, **61**: S283–S299. doi:10.1002/lno.10307.

Jones, F.W., Majorowicz, J.A., Dietrich, J., and Jessop, A.M. 1990. *Geothermal gradients and heat flow in the Beaufort-Mackenzie Basin, Arctic Canada*. Pure and Applied Geophysics, PAGEOPH, **134**(3): 473–483. doi:10.1007/BF00878743.

Kim, H.S., Cho, G.C., Lee, J.Y., and Kim, S.J. 2013. *Geotechnical and geophysical properties of deep marine fine-grained sediments recovered during the second Ulleung Basin Gas Hydrate expedition, East Sea, Korea*. Marine and Petroleum Geology, **47**: 56–65. Elsevier Ltd. doi:10.1016/j.marpetgeo.2013.05.009.

Klauda, J.B. and Sandler, S.I. 2005. *Global distribution of methane hydrate in ocean sediment*. Energy and Fuels, **19**(2): 459–470. doi:10.1021/ef049798o.

Majorowicz, J.A. and Embry, A.F. 1998. *Present heat flow and paleo-geothermal regime in the Canadian Arctic margin: analysis of industrial thermal data and coalification gradients*. Tectonophysics, **291**(1–4): 141–159. doi:10.1016/S0040-1951(98)00036-5.

Muraoka, M., Ohtake, M., Susuki, N., Yamamoto, Y., Suzuki, K., and Tsuji, T. 2014. *Thermal properties of methane hydrate-bearing sediments and surrounding mud recovered from Nankai Trough wells*. Journal of Geophysical Research: Solid Earth,: 8021–8033. doi:10.1002/2014JB011324.

Nixon, M.F. and Grozic, J.L.H. 2007. *Submarine slope failure due to gas hydrate dissociation: a preliminary quantification*. Canadian Geotechnical Journal, **44**(3): 314–325. doi:10.1139/t06-121.

Priest, J.A., Clayton, C.R.I., and Rees, E.V.L. 2014. *Potential impact of gas hydrate and its dissociation on the strength of host sediment in the Krishna-Godavari Basin*. Marine and Petroleum Geology, **58**(PA): 187–198. Elsevier Ltd. doi:10.1016/j.marpetgeo.2014.05.008.

Priest, J.A. and Grozic, J.L.H. 2016. *Stability of fine-grained sediments subject to gas hydrate dissociation in the arctic continental margin*. Advances in Natural and Technological Hazards Research, **41**: 427–436. doi:10.1007/978-3-319-20979-1_43.

Reagan, M.T., Moridis, G.J., Elliott, S.M., and Maltrud, M. 2011. *Contribution of oceanic gas hydrate dissociation to the formation of Arctic Ocean methane plumes*. Journal of Geophysical Research, **116**(C09014): 1–11. doi:10.1029/2011JC007189.

Rees, E.V.L., Priest, J.A., and Clayton, C.R.I. 2011. *The structure of methane gas hydrate bearing sediments from the Krishna-Godavari Basin as seen from Micro-CT scanning*. Marine and Petroleum Geology, **28**(7): 1283–1293. Elsevier Ltd. doi:10.1016/j.marpetgeo.2011.03.015.

Ruppel, C.D. and Kessler, J.D. 2017. *The interaction of climate change and methane hydrates*. Reviews of Geophysics, **55**(1): 126–168. doi:10.1002/2016RG000534.

Sloan, E.D. 1998. *HYDRATE PREDICTION PROGRAM: HYDOFF*. Center for Hydrate Research, Department of Chemical and Petroleum-Refining Engineering, Colorado School of Mines, Golden, CO 80401.

Taylor, A.E., Dallimore, S.R., Hill, P.R., Issler, D.R., Blasco, S., and Wright, F. 2013. *Numerical model of the geothermal regime on the Beaufort Shelf, arctic Canada since the Last Interglacial*. Journal of Geophysical Research: Earth Surface, **118**(4): 2365–2379. doi:10.1002/2013JF002859.

Vadakkepuliyambatta, S., Skeie, R.B., Myhre, G., Dalsoren, S.B., Schmidbauer, N., Myhre, C.L., and Mienert, J. 2017. *Climatic impact of Arctic Ocean methane hydrate dissociation in the 21 st -century*. Earth System Dynamics,: 1–27.

Waite, W.F. 2007. *Thermal Properties of Methane Gas Hydrates*. USGS, (July): 1–2. doi:10.1063/1.2194481.Waite.

Waite, W.F., Santamarina, J.C., Cortes, D.D., Dugan, B., Espinoza, D.N., Germaine, J., Jang, J., Jung, J.W., Kneafsey, T.J., Shin, H., Soga, K., Winters, W.J., and Yun, T.S. 2009. *Physical properties of hydrate-bearing sediments*. Reviews of Geophysics, **47**(4): 1–38. doi:10.1029/2008RG000279.

Williams, P.J. and Smith, M.W. 2009. *The Ground Thermal Regime*. *In* The Frozen Earth: Foundamental of Geology. Cambridge University Press. pp. 83–121. doi:10.1017/CBO9780511564437.005.

Yun, T.S., Fratta, D., and Santamarina, J.C. 2010. *Hydrate-bearing sediments from the Krishna-Godavari basin: Physical characterization, pressure core testing, and scaled production monitoring*. Energy and Fuels, **24**(11): 5972–5983. doi:10.1021/ef100821t.